Electroosmotic flow reversal outside glass nanopores: Supplementary Information

Nadanai Laohakunakorn,[†] Vivek V. Thacker,[†] Murugappan Muthukumar,[‡] and Ulrich F. Keyser[*,†]

Cavendish Laboratory, University of Cambridge, Cambridge CB3 0HE, UK, and Department of Polymer Science and Engineering, University of Massachusetts Amherst, 120 Governors Drive, Amherst, MA 01003, USA

E-mail: ufk20@cam.ac.uk

[*]To whom correspondence should be addressed
[†]University of Cambridge
[‡]University of Massachusetts Amherst

Supplementary Figure S1

P values as a function of salt concentration for three different pore sizes; (A), (B), and (C) show the experimental results, while (D), (E), and (F) show the simulation results. The qualitative features of flow rectification asymmetry, flow reversal, and pore size dependence of the crossover point are faithfully captured by the simulations. The magnitudes of P are similar but not exact; however the increasing magnitude of P as a function of pore size is also captured. For 15 and 150 nm pores, P increases faster at low salt in the simulations compared to in experiments; this is most likely due to the constant surface charge assumption in the simulations. In reality at low salt the surface charge is reduced due to counterion adsorption. The available computer memory sets a low salt limit for the simulations, due to the finer mesh required to simulate situations with large nonlinearities: this prevents us from simulating the entire range of salt concentrations measured experimentally. For the 1000 nm pore, this limitation means that we do not see complete flow reversal behaviour (although the decrease in the positive branch is already observed at 0.1 mM). The behaviour of the positive branch in the case of the 15 nm capillary differs from the 150 and 1000 nm capillaries in that it does not contain a maximum; we expect, however, that the maximum is present, albeit at higher salt concentrations which are inaccessible experimentally, as the forces become too small to be resolved by our setup (which has a force resolution of ~ 0.5 pN).

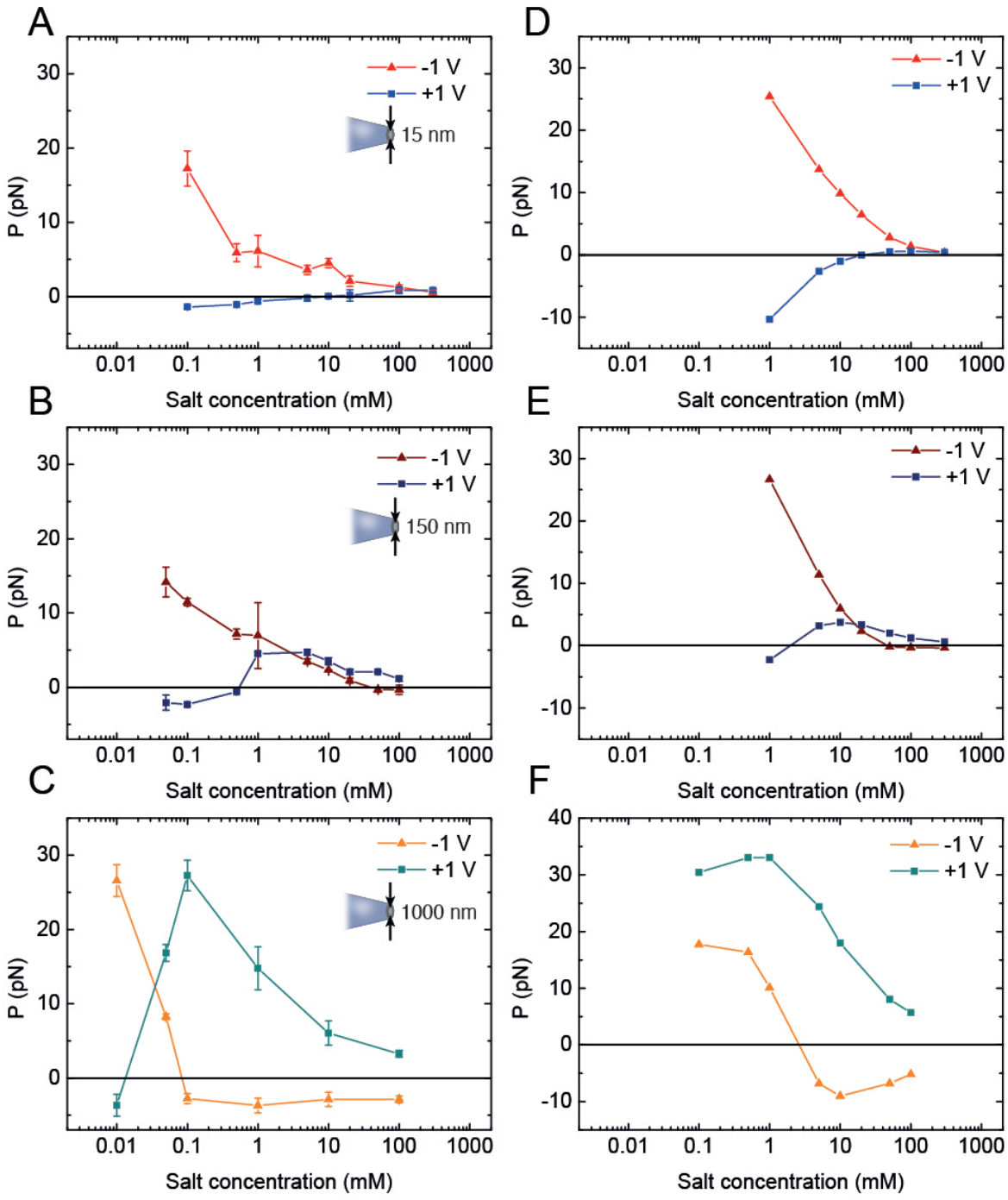
A
B
C
D
E
F
-1 V
+1 V
15 nm
150 nm
1000 nm
P (pN)
Salt concentration (mM)
0.01
0.1
1
10
100
1000

Supporting Information S2

Here we give a full description of the simulation procedure. The PNP equations are given by

$$\boldsymbol{J}_i = -D_i \nabla c_i - \frac{D_i}{RT} z_i e N_A c_i \nabla \phi(\boldsymbol{r}) + c_i \boldsymbol{u} \tag{1}$$

$$\nabla^2 \phi(\boldsymbol{r}) = -\frac{\rho_e(\boldsymbol{r})}{\epsilon_0 \epsilon_r}, \tag{2}$$

which are combined with the Stokes equation

$$\mu \nabla^2 \boldsymbol{u} = \rho_e(\boldsymbol{r}) \nabla \phi(\boldsymbol{r}) + \nabla p. \tag{3}$$

First, eqs 1 and 2 are solved neglecting convection (the $c_i \boldsymbol{u}$ term). This outputs $\boldsymbol{J}_i$ and c_i, and hence $\rho_e(\boldsymbol{r})$, and $\phi(\boldsymbol{r})$. $\phi(\boldsymbol{r})$ and $\rho_e(\boldsymbol{r})$ are the inputs for the body force in the Stokes equation, which is solved in a second step to produce $u(\boldsymbol{r})$ and $p(\boldsymbol{r})$.

The geometry used is a 2D-axisymmetric geometry with a conical pore parameterised by two values α and β, the taper angles of the inner and outer walls respectively. We use values of $\alpha = 5°$ and $\beta = 10°$; these values are representative of the actual taper angles as measured using the SEM. The two segements describing the walls meet at a virtual origin, but the physical walls are truncated at a given pore radius R. The offset distance of the pore to the origin is $L_0 = R/\tan(\alpha)$. The reservoir is spherically symmetric and centred about the virtual origin, which means that the walls intersect the reservoir boundary at right angles. The reservoir size is $20L_0$, which is just about large enough to mimic infinity. The motivation for using a spherical reservoir is that the closest distance of the real capillary to any surface is around 250 μm, and so from the point of view of the nanpore the reservoir is essentially isotropic and symmetric in all directions.

Sharp corners D and E are rounded with a filleting radius of $R/10$. The reference (inner) electrode F'G has a radius of 2 nm. The walls are modelled as a glass dielectric with $\epsilon_r = 4.2$, and the fluid is water with $\epsilon = 80$.

A refined mesh was used with mesh control domains situated about the pore entrance (size $10R$), and at the two corners C and F where the glass walls meet the reservoir boundary (size $5R$). Inside the control domains the mesh is heavily refined with maximum element sizes of 0.2 nm. Outside these domains a predefined mesh was used optimized for fluid dynamics; the maximum element size is around 50 nm. On the wall surface a 9-level boundary layer was created, with the first layer thickness equal to approximately $\lambda_D/3$ and a maximum growth rate of 20% between layers. The key to running the simulation successfully is this mesh design, as it has significant effects on convergence and numerical stability.

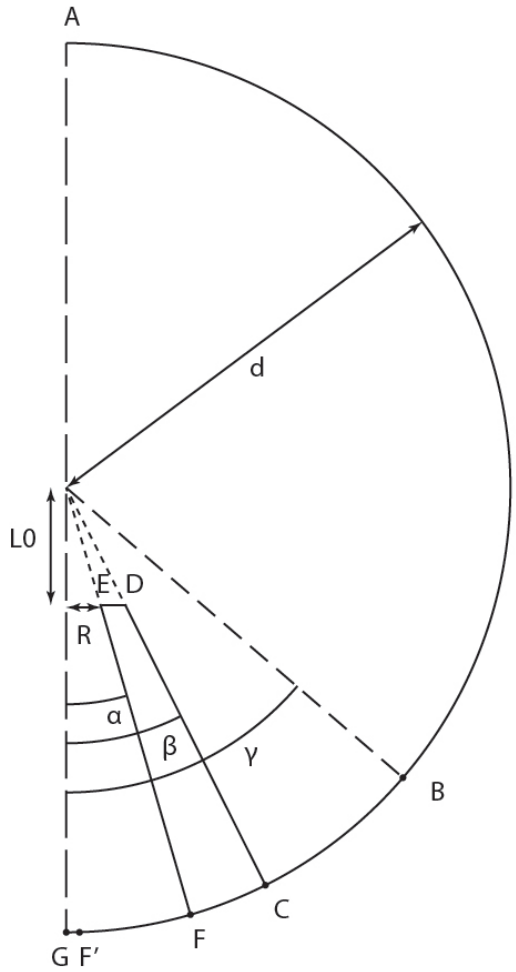

For the boundary conditions, we divide the problem into two halves: first we solve the PNP equations (eq. 1, 2) along the 1D boundary GF'FCB. The boundary is parameterised

by the angle γ, which can is set to a value large enough that the point B mimics an infinite distance away from the wall at C. The following boundary conditions are used:

- Poisson: surface charge σ at F and C, potential $\phi = V_0$ at F' and $\phi = 0$ at B. ϕ is constant and equal to V_0 on GF'.
- Nernst-Planck: concentration $c = c_0$ at F' and B, no flux at F and C. The concentration is constant and equal to c_0 on GF'.

The solution of this problem is the electric potential ϕ_{1D} and concentration $c_{i,1D}$ for both species along the boundary, which are used as Dirichlet boundary conditions for the 2D PNP equations. We also obtain the fluid pressure on CB using

$$p = 2N_A c_0 k_B T \left[\cosh\left(\frac{e(\phi - V_0)}{k_B T}\right) - 1\right] \tag{4}$$

and on F'F,

$$p = 2N_A c_0 k_B T \left[\cosh\left(\frac{e(\phi)}{k_B T}\right) - 1\right]. \tag{5}$$

This sets a Dirichlet boundary condition p_{1D} for the Stokes equation.

After the 1D problem has been solved we then solve the full 2D problem using the following BCs:

- Poisson: surface charge σ on FEDC, potential $\phi = 0$ on AB, $\phi = \phi_{1D}$ on GF'FCB.
- Nernst-Planck: concentration $c_i = c_0$ on AB, $c_i = c_{i,1D}$ on GF'FCB.
- Stokes: pressure $p = 0$ on GF' and AB, $p = p_{1D}$ on GF'FCB using COMSOL's 'normal boundary stress' condition.

The 1D solution is computed using a fully coupled solver. The 2D solution uses a segregated solver which solves the PNP equations in the first step, and the Stokes equation in the second. The convergence criterion is a tolerance of 10^{-3}. For discretization we use quadratic elements for the PNP equations, and P2+P1 for Stokes (second order velocity, first order

pressure). The solution time is roughly 500 seconds on a machine running a 4-core 3.33 GHz Intel i7 processor, with 12GB RAM.

For cases where the nonlinearity is large (for instance, when high voltages are used) convergence is achieved using load ramping: the surface charge is slowly increased, with the final solution for each run used as the initial condition for the subsequent run. This method takes roughly 2,500 seconds to run, and using this method we are able to achieve convergence in all cases.

To assure the validity of our method we can compute some benchmark results, shown below. Here we apply the same simulation method to compute the solution for an infinite cylinder; points represent simulation results, and solid lines the analytic Debye-Hückel solutions. At high salt we see that the simulations faithfully reproduce the analytic solutions, while at low salt there is a discrepancy, due to the breakdown of the Debye-Hückel approximation.

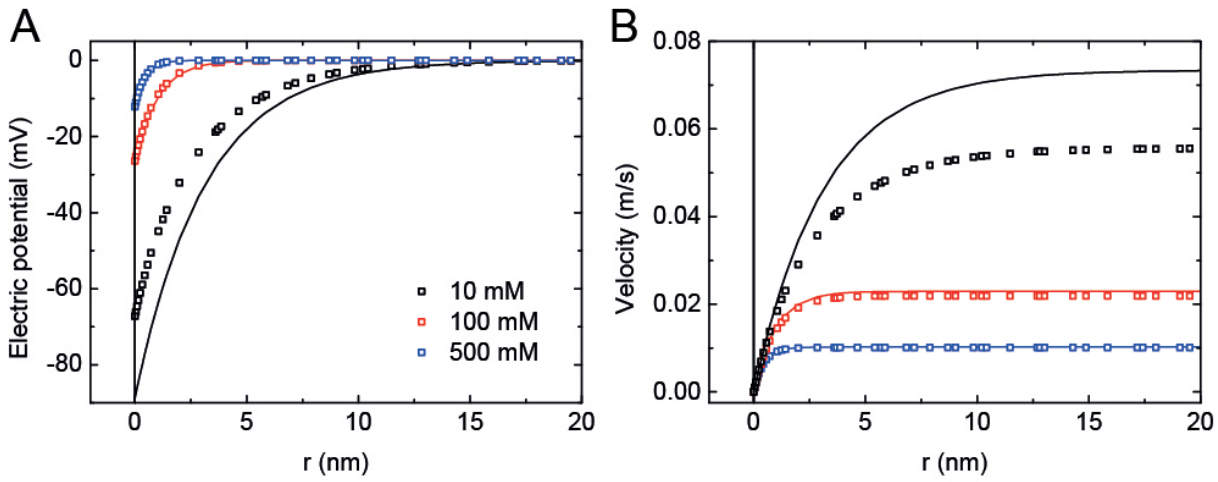

Supplementary Figure S3

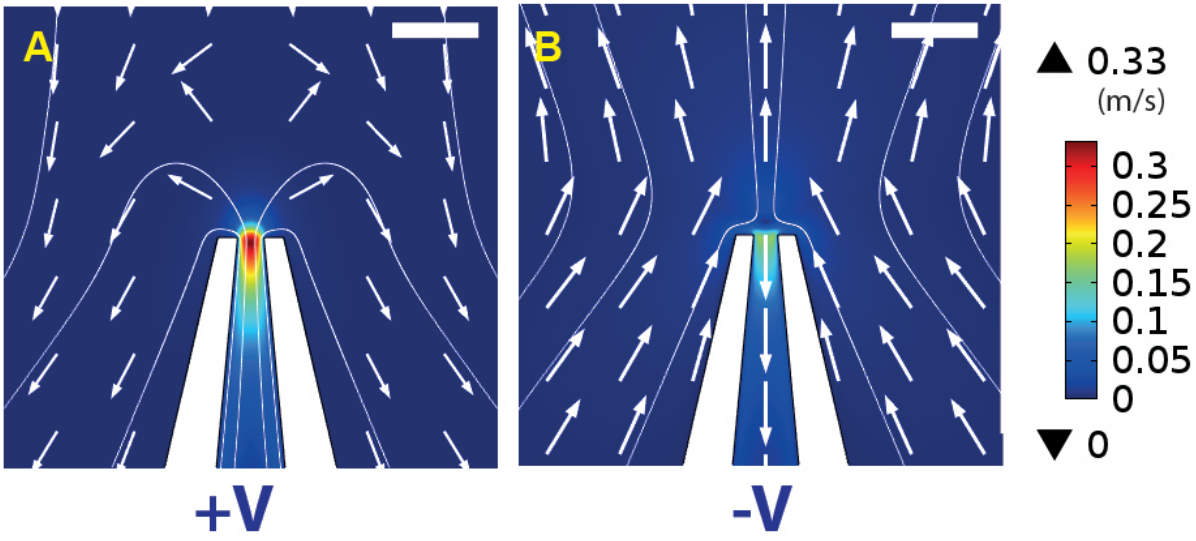

The direction of electroosmotic flow inside the pore always exhibits the expected behaviour, even at low salt concentrations (when the external flow field is reversed). Here we show simulation results for a 15 nm pore at 10 mM, under applied voltages of ± 1 V. The scale bar represents 50 nm.

Supplementary Figure S4

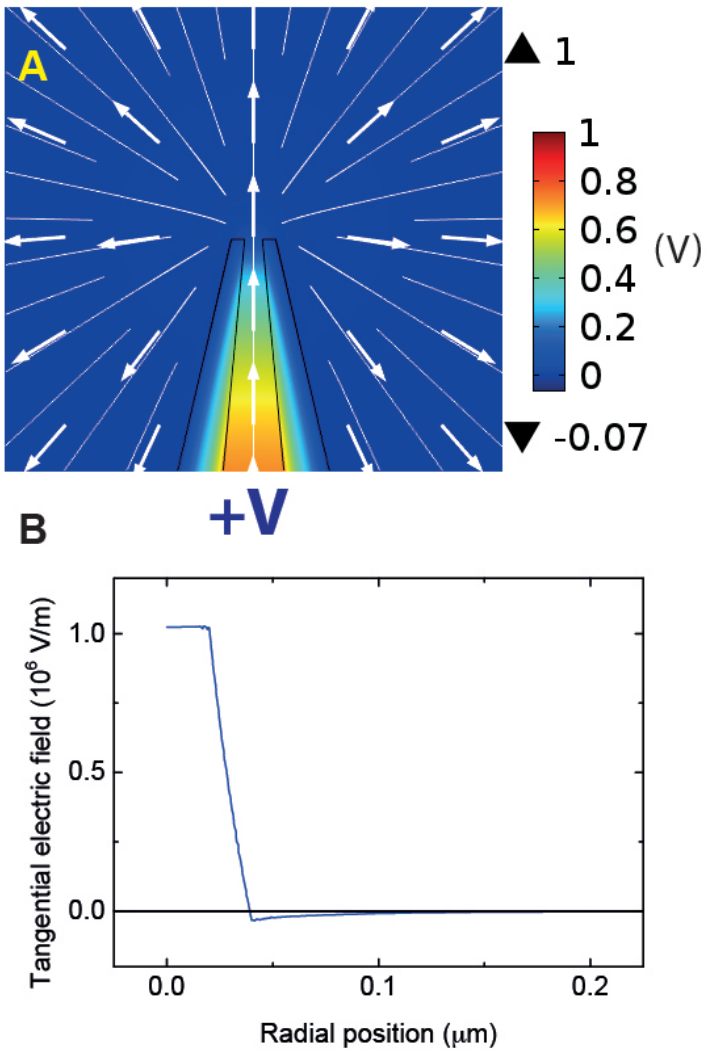

(A) The conical pore behaves like a point source of electric fields; this is expected from the symmetry of the reservoir, as the closest surface to the pore is the glass cover slide, ~ 250 μm away, and the reservoir is essentially infinite and isotropic from the point of view of the pore. Here arrows indicate direction (not magnitude) of the electric field outside a 15 nm diameter pore, and the colours indicate electric potential. The electric field points approximately in opposite directions along the inner and outer walls, motivating the analytic model of the infinite cylinder with opposing electric fields. (B) The tangential electric field

inside and outside a finite cylindrical pore. The field inside is approximately an order of magnitude greater than the field outside, and in the opposite direction.

Supplementary Figure S5

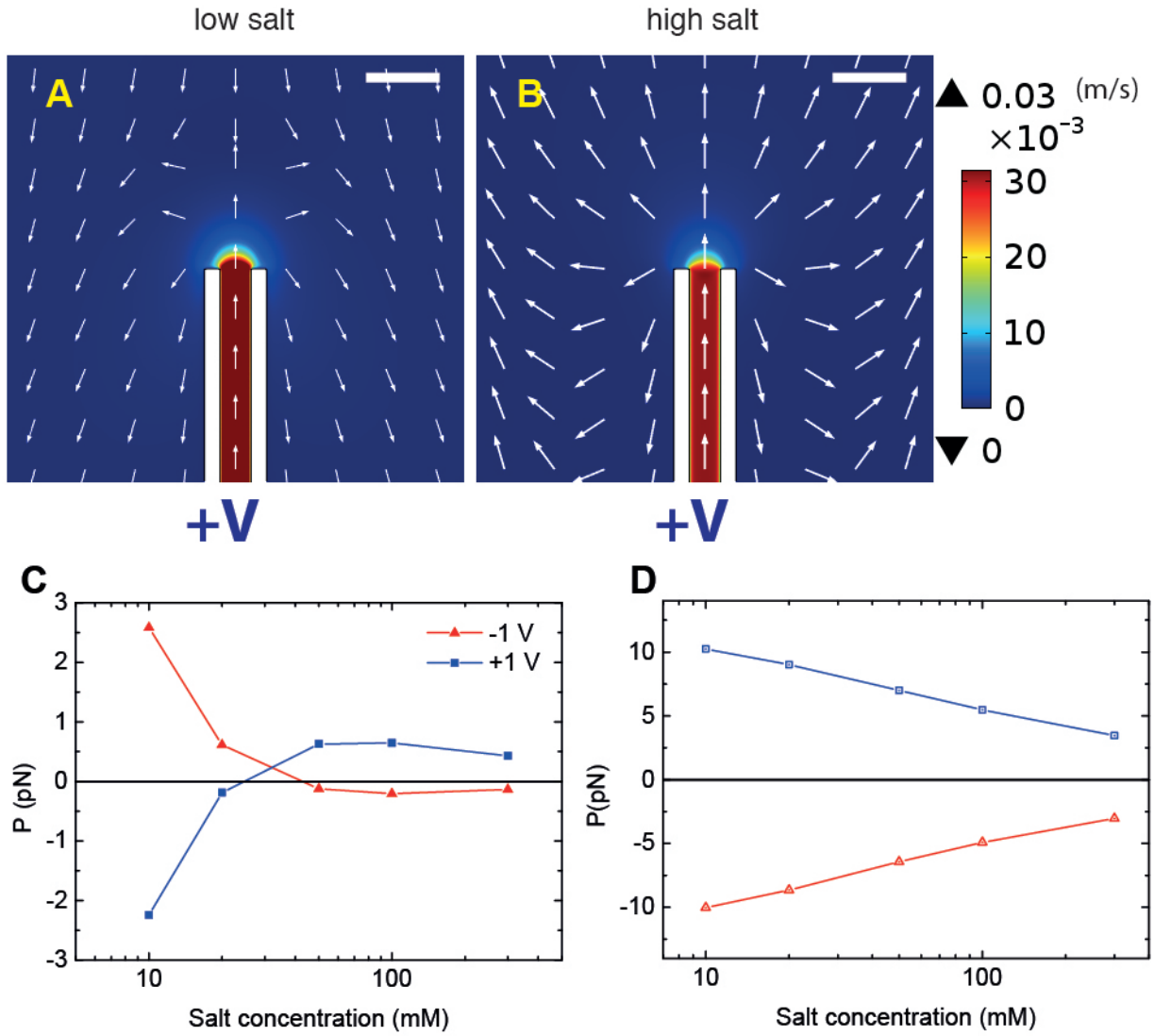

Simulations were also carried out for a finite cylindrical pore of diameter 40 nm; here, low salt corresponds to 10 mM, and high salt to 50 mM. Scale bars represent 100 nm. (A), (B), and (C) show that the flow reversal behaviour is preserved, demonstrating that the conical geometry is not necessary. (D) shows the effect of running the simulation without charges on the outer wall; the flow reversal behaviour is lost in this case, suggesting that the outer wall plays a vital role in generating flow reversal.